Science of the Total Environment 661 (2019) 35–47

Contents lists available at ScienceDirect

Science of the Total Environment

journal homepage: www.elsevier.com/locate/scitotenv

Verification of satellite ozone/temperature profile products and ozone effective height/temperature over Kunming, China

Haoyue Wang [a,b], Suying Chai [b,c], Xiao Tang [d], Bin Zhou [a,e,*], Jianchun Bian [f], Holger Vömel [g], Ke Yu [h], Weiguo Wang [b,**]

[a] Department of Environmental Science and Engineering, Institute of Atmospheric Sciences, Shanghai Key Laboratory of Atmospheric Particle Pollution and Prevention (LAP3), Fudan University, Shanghai, China
[b] Department of Atmosphere Science, Yunnan University, Kunming, China
[c] Yunan Institute of Environmental Science, Kunming, China
[d] Institute of Atmospheric Physics, Chinese Academy of Sciences, State Key Laboratory of Atmospheric Boundary Layer Physics and Atmospheric Chemistry (LAPC), Beijing, China
[e] Shanghai Institute of Eco-Chongming (SIEC), No. 3663 Northern Zhongshan Road, Shanghai, China
[f] Key Laboratory of Middle Atmosphere and Global Environment Observation, Institute of Atmospheric Physics, Chinese Academy of Sciences, Beijing, China
[g] Earth Observing Laboratory, National Center for Atmospheric Research, Boulder, CO, USA
[h] Meteorological Information Center of Yunnan Province, Kunming, China

HIGHLIGHTS

- MLS and AIRS data in the UTLS region are not sensitive enough and have large deviations from ECC values.
- Sensitivity of AIRS temperature products is greater in the troposphere than stratosphere.
- Sensitivity of total ozone change to effective temperature change varies with season.

GRAPHICAL ABSTRACT

(a) Comparison between MLS, AIRS and ECC ozone profiles; (b) relative deviation between MLS and ECC and AIRS and ECC over Kunming on March 5, 2014.

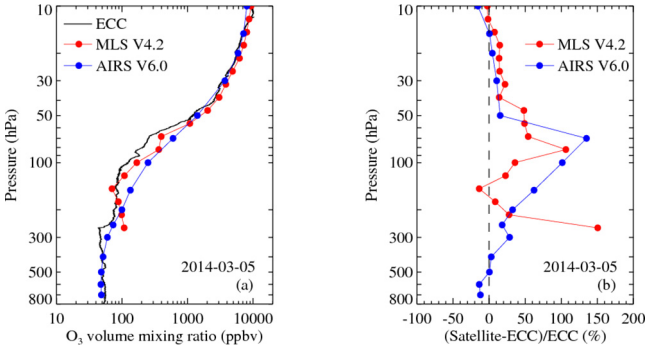

ARTICLE INFO

Article history:
Received 7 October 2018
Received in revised form 28 December 2018
Accepted 13 January 2019
Available online 15 January 2019

Editor: Pavlos Kassomenos

Keywords:
MLS
AIRS
Sounding experiment

ABSTRACT

Ozonesonde data from November 2013 to April 2015 over Kunming, China are used to verify ozone and temperature profile retrievals from two spaceborne instruments, the version 4.2 product from the Microwave Limb Sounder (MLS) on the NASA Aura satellite and the version 6.0 product from the Atmospheric Infrared Sounder (AIRS) on the NASA Aqua satellite. We calculated and compared the ozone effective height H_{eff} and effective temperature T_{eff}, which are two important parameters in ground-based total ozone retrieval through the use of various profile datasets. This is used to verify the accuracy of the operative values ($H_{eff(0)} = 23$ km, $T_{eff(0)} = -46.3$ °C (or −45 °C)) from the World Meteorological Organization. The results show that the deviation of MLS and AIRS ozone profiles from ozone sounding data has significant oscillation and scatter in the upper troposphere and lower stratosphere. The average difference of MLS at 82.5 hPa is (80.5 ± 65.1) %, and that of AIRS at 70 and 100 hPa are (105.6 ± 74.9) % and (107.0 ± 67.8) %, respectively. The two satellite temperature profiles have

* Correspondence to: B. Zhou, Department of Environmental Science and Engineering, Institute of Atmospheric Sciences, Shanghai Key Laboratory of Atmospheric Particle Pollution and Prevention (LAP[3]), Fudan University, Shanghai, China.
** Correspondence to: W. Wang, Department of Atmosphere Science, Yunnan University, Kunming, China.
E-mail addresses: binzhou@fudan.edu.cn (B. Zhou), wangwg@ynu.edu.cn (W. Wang).

https://doi.org/10.1016/j.scitotenv.2019.01.145
0048-9697/

Ozone and temperature profile
Ozone effective height and effective temperature

differences within ±3 °C and can effectively describe the vertical distribution and variation of temperature. When calculating the H_{eff} and T_{eff}, upper stratospheric data missing from the sounding data must be filled in by the satellite profile data; otherwise the calculated results will show large errors of 3.2 km and 3.3 °C. The H_{eff} and T_{eff} at Kunming are respectively 24.36 to 25.51 km and −48.3 to −43.6 °C. The operational H_{eff} and T_{eff} used at Kunming ozone observation station clearly do not conform to the actual situation and must be corrected.

1. Introduction

Ozone is a trace gas in the earth's atmosphere, and 90% is in the stratosphere and only ~10% in the troposphere. Stratospheric ozone can be transported into the troposphere (Wang et al., 2006, 2010). Stratospheric ozone strongly absorbs ultraviolet radiation from the sun and plays a role in protecting the biosphere, but tropospheric ozone is a greenhouse gas and an important component of air pollution. With the development of industrialization and the influence of human factors, the spatial and temporal distributions of ozone profiles in different regions change constantly. The impacts of this change on the ecology, environment and climate are complex (Shang et al., 2017; Stergiopoulou et al., 2018; Miller et al., 2015; Li et al., 2018). Correlation between ozone profile changes and environmental air pollution is consistent with influences of the ozone profile obtained by photochemical theory (Gao et al., 2017; Wang et al., 2017). Local meteorological conditions have a major influence on the spatial and temporal variation of ozone and its precursors, and can cause fluctuation of the diurnal variation of the ozone profile. The ozone profile variation also reflects the basic characteristics of the atmospheric meteorological profile, which can be used to assess the transport and diffusion of ozone. However, seasonal variation of the vertical distribution of ozone is greater than that of local meteorological conditions (Dueñas et al., 2002; Elminir, 2005), so ozone has always been a difficult and popular problem issue in research. Therefore, measurement of the vertical distribution of ozone is of great theoretical significance and practical value in the correction of data in the environmental, ecological and atmospheric science, as well as in atmospheric remote sensing.

Detection of the vertical distribution of ozone mainly includes the direct measurement of ozonesonde and aircraft, as well as the telemetry inversion of satellite data and ground-based measurements. As a reference for the verification of satellite remote sensing products, atmospheric sounding techniques have been developed to maturity. The ozone detector based on an electrochemical concentration cell (ECC) has been widely used (Komhyr et al., 1995). This is because the high quality of ozone data from soundings is better than that of satellite inversion data, which has promoted the development of satellite inversion technology. The microwave limb sounder (MLS) on the Aura satellite and atmospheric infrared sounder (AIRS) on the Aqua satellite are two of the main sensors that measure atmospheric vertical distributions by remote sensing. Satellite products must be validated before use. The verification method mainly includes the use of direct measurements of ozonesonde and aircraft (Divakarla et al., 2006, 2008; Pittman et al., 2009) or comparison between reanalysis data and various satellite products (Froidevaux et al., 2006, 2008; Schwartz et al., 2008; Liu et al., 2010). At present, there has been little work on the verification of MLS and AIRS ozone products in China. Bian et al. (2007) used GPSO3 sounding data to verify MLS version 1.5 and AIRS version 4.0 ozone profiles over Beijing. The result shows that the two satellite products can reflect the distribution and variation of ozone in the upper troposphere and lower stratosphere (UTLS). Yan et al. (2015) verified MLS ozone profiles over the Tibetan Plateau and adjacent areas.

The ozone effective height H_{eff} is defined as the ozone-weighted mean height from the ground to the top of the atmosphere and is an important parameter for ground-based total ozone retrieval and calculation of the ozone air mass (Thomas and Holland, 1977; Bernhard et al., 2005). The ozone effective temperature T_{eff} is defined as the ozone-weighted mean temperature from the ground to the top of the atmosphere and is an important parameter to calculate the ozone effective absorption coefficient and measure total ozone (Scarnato et al., 2009; Redondas et al., 2014). There will be large error in calculating the effective height and effective temperature of ozone using high-resolution sounding data without upper stratospheric data. This error will produce significant error in total ozone inversion, so satellite observation data of the upper stratosphere must be supplemented. Therefore, it is necessary to consider the actual height distribution of ozone layer at specific time and space points to accurately determine the total amount of ozone. In 1983, Klenk et al. used sounding and satellite data to splice the ozone profile of 40–0.7 hPa, but ignored ozone profile of the ground ~40 hPa and above 0.7 hPa. In 1985, according to Ground-Based and satellite observation data at 45°N, Bhartia et al. again jointed and redefined ozone and temperature profiles from the ground to ~60 km (referred to as the 1985 standard profile). Recommended by the International Ozone Commission (IO3C), on January 1, 1992, the World Meteorological Organization (WMO) took the effective height and effective temperature of ozone calculated by the 1985 standard profile as standard values of ground observation inversion. Therefore, in the standard inversion algorithm of Dobson and Brewer, fixed ozone effective height and effective temperature parameters are used as the calibration system. In fact, variation of the ozone and temperature profiles with longitude, latitude and season at different stations should be considered to obtain more accurate Dobson and Brewer parameters (Scarnato et al., 2009). Kunming ozone observation station (25.03°N, 102.68°E, altitude 1917 m) is station number 209 of the Global Ozone Observation System GO_3OS. The operational standard ozone effective height $H_{eff(0)}$ is 23.0 km and the effective temperature $T_{eff(0)}$ is −46.3 or −45 °C, used by the Dobson (D003) and Brewer MKIII (B198) spectrometer at Kunming. These two operational parameters from WMO are empirical. Further testing is needed to determine whether these values correspond to reality. The satellite profile data will be used to calculate H_{eff} and T_{eff}, so they must be validated first in this study.

Kunming station is on a low-latitude plateau to the southeast of the Qinghai–Tibet Plateau and an important channel of exchange between troposphere and stratosphere. In order to obtain seasonal ozone profiles over Kunming in the Asian monsoon region, integrated sounding experiments using the electrochemical concentration cell (ECC) and 403-MHz iMet-1 meteorological radiosonde were carried out from November 2013 to April 2015. To provide application references, we used ozone and temperature sounding data to verify the MLS version 4.2 and AIRS version 6.0 remote sensing products. Then, using satellite and sounding profile data, we verified the operational $H_{eff(0)}$ and $T_{eff(0)}$ used by the spectrometer at Kunming station.

2. Data and methods

2.1. Sounding data

A one-year ozone sounding experiment was carried out from November 2013 to November 2014 at the Kunming ozone observatory, and supplementary observation was conducted in the first half of 2015. Table 1 shows sounding data heights and coincidences of MLS (AIRS) with the in-situ profiles. The MLS (AIRS) profiles coincident with the in-situ profiles were selected from the smallest space and

time interval between the sonde launches and MLS (AIRS) overpasses (Table 1).

The experiment was conducted using the 403-MHz iMet-1 meteorological radiosonde produced by International Met Systems Group (InterMet). The detection range of pressure is 1070–2 hPa. The resolution is 0.01 hPa and the accuracy is ±1.8 hPa (>400 hPa) and ± 0.5 hPa (400–2 hPa). The detection range of temperature is −95 to 50 °C. The resolution is 0.01 °C and the accuracy is ±0.3 °C.

The ECC ozonesonde is used to determine ozone concentration by the electric current generated by the electrochemical reaction between ozone and potassium iodide solution (Komhyr et al., 1995). According to the experimental record, the vertical resolution is 4–7 m. Studies show that the uncertainty of ECC measurement is about 10% in the troposphere, 5% in the stratosphere to 10 hPa, and 5–25% from 10 to 3 hPa (Kerr et al., 1994; Bodeker et al., 1998; World Climate Research Programme, 1998; Borchi et al., 2005; Smit et al., 2007; Thompson et al., 2007a, 2007b, 2007c). Therefore, only data below the 10 h Pa level of the ECC ozone profile (~30 km) were used.

2.2. MLS products

The MLS is one of the major sensors aboard the sun-synchronous polar satellite Aura. It can provide data for vertical profiles of temperature and a variety of trace gases (such as ozone and water vapor) from the upper troposphere to mesosphere. The latest data released with Aura-MLS version 4.2 has a modified processing scheme for cloud signals during the inversion process, substantially reducing spurious data in cloud regions. The quality of cloud region data in the upper troposphere is improved relative to earlier version 3. We used the level-2 ozone and temperature profile inversion products of NASA GES DISC version 4.2, which provides 3494 global profiles daily. The height range of ozone and temperature profiles is 261–0.1 hPa. In this range, the vertical and horizontal resolutions of ozone are 2.5–4 and 300–500 km, respectively. The vertical and horizontal resolutions of temperature are 3.5–8 and 165–170 km, respectively.

2.3. AIRS products

The AIRS is one of the sensors aboard the sun-synchronous near-polar satellite Aqua, which can provide profile data of temperature, ozone and water vapor from the ground to mesosphere. The data currently released by Aqua-AIRS includes versions 5 and 6. Because the basic inversion method has not changed, there is little difference between data of the two versions. However, there are some improvements to the data of version 6, such as a general reduction of uncertainty and improvement of cloud-top features. As Divakarla et al. (2006) pointed out, the false long-term trend of bias has been mitigated. We used the secondary ozone and temperature profile inversion products of NASA GES DISC version 6, which provides 324,000 global profiles daily. The height range of ozone and temperature profiles is 1100–0.1 hPa, which is divided into 28 layers. The vertical resolution is lower than that of MLS and the horizontal resolution is ~45 km, better than that of MLS.

2.4. Methods

Because the vertical resolution of satellite data is much less than that of sounding data, the vertical resolution of the latter data must be reduced in order to match the two. Livesey et al. (2015) recommended sounding data interpolation for the validation of MLS data. In this way, the errors of satellite products can be recognized effectively and the actual accuracy of those products can be shown. Lagrange linear interpolation was used in our work. This method has been widely used in the verification of satellite profile products to reduce the vertical resolution of the sounding data to match that of the satellite data (Berthet et al., 2013). Some scholars have used the least squares and average kernel function methods to reduce the vertical resolution of ozone sounding data for comparison with satellite data. Jiang et al. (2007) pointed out that there was little difference between the two methods in reducing the vertical resolution of ozone sounding data. Moreover, the comparison result between MLS and sounding data was not sensitive to the selection of either method.

The purpose of comparing various satellite and sounding data is to more effectively apply the observation data of different satellites. The spatial and temporal resolutions of MLS are completely different from AIRS, i.e., those of MLS are low and those of AIRS relatively high. During the comparative analysis, MLS and AIRS satellite data matching the sounding data were selected from profiles closest to the sounding site and with the shortest time difference at observation time. The horizontal resolution of MLS products is low, because those products mainly depict levels above the upper troposphere and, at these heights, the distribution of ozone level changes little. We referred to Vömel et al. (2007) and Yan et al. (2015) and, for comparison, we chose the MLS profile within ±5° latitude and ±8° longitude of the sounding site, and a period within ±12 h for sounding satellite data. Such spatial and temporal resolution has little influence on the comparison results (Bian et al., 2007). Because the horizontal resolution of AIRS products is greater than that of MLS, the selection criteria of latitude and longitude and time are ±0.5° to ±1.0° and ±12 h, respectively. In addition, the selection of specific satellite data strictly followed corresponding quality control documents.

Table 1
Heights of sounding data and coincidences of MLS (AIRS) with in-situ profiles over Kunming from November 2013 to April 2015.

No.	Date	Height (hPa/km)	MLS coincidence	AIRS coincidence	No.	Date	Height (hPa/km)	MLS coincidence	AIRS coincidence
1	2013/11/26	2.51/36.01	Yes	Yes	19	2014/07/15	2.63/35.67	Yes	Yes
2	2013/12/04	2.51/35.22	Yes	Yes	20	2014/07/25	2.51/36.32	Yes	Yes
3	2013/12/20	2.89/36.91	Yes	Yes	21	2014/08/05	2.52/34.80	Yes	Yes
4	2013/12/29	2.51/36.36	Yes	Yes	22	2014/08/15	2.51/36.52	Yes	Yes
5	2014/01/16	2.51/35.75	Yes	Yes	23	2014/08/25	2.51/38.00	Yes	Yes
6	2014/01/26	2.51/36.36	Yes	Yes	24	2014/09/05	2.51/37.61	Yes	Yes
7	2014/02/10	19.49/26.18	Yes	Yes	25	2014/09/15	2.51/37.80	Yes	Yes
8	2014/03/05	2.52/36.29	Yes	Yes	26	2014/09/25	2.84/37.01	Yes	Yes
9	2014/03/25	8.85/31.69	Yes	No	27	2014/10/05	2.52/34.04	Yes	Yes
10	2014/04/15	2.51/38.96	Yes	Yes	28	2014/10/15	3.08/35.28	Yes	Yes
11	2014/04/25	2.51/36.03	Yes	Yes	29	2014/10/25	2.51/36.86	Yes	Yes
12	2014/05/05	2.51/34.69	Yes	Yes	30	2014/11/05	2.51/37.56	Yes	Yes
13	2014/05/15	2.51/35.12	Yes	Yes	31	2014/11/15	2.51/35.05	Yes	Yes
14	2014/05/25	2.52/35.46	Yes	Yes	32	2015/01/10	2.51/36.51	Yes	Yes
15	2014/06/05	68.35/18.70	Yes	Yes	33	2015/02/05	2.53/36.58	Yes	Yes
16	2014/06/15	2.51/35.32	Yes	Yes	34	2015/02/25	2.51/36.11	Yes	Yes
17	2014/06/25	2.51/35.21	Yes	Yes	35	2015/03/25	2.53/36.93	Yes	Yes
18	2014/07/05	2.51/34.83	Yes	Yes	36	2015/04/05	11.49/29.15	Yes	Yes

The comprehensive effect of the vertical distribution of ozone and temperature on the ozone effective absorption coefficient can be expressed by the effective height H_{eff} and effective temperature T_{eff}, i.e., ozone-weighted mean height and temperature (Thomas and Holland, 1977):

$$Heff = \frac{\int_{z_0}^{\infty} z\rho(z)\mathrm{d}z}{\int_{z_0}^{\infty} \rho(z)\mathrm{d}z}$$
$$Teff = \frac{\int_{z_0}^{\infty} T(z)\rho(z)\mathrm{d}z}{\int_{z_0}^{\infty} \rho(z)\mathrm{d}z}, \quad (1)$$

where z is height, z_0 is station elevation, $T(z)$ is Kelvin temperature, and $\rho(z)$ is ozone density.

3. Comparison of ozone/temperature profiles

3.1. Deviation of individual cases

Fig. 1 shows a comparison of ECC, AIRS and MLS ozone profiles over Kunming on March 5, 2014. As shown in Fig. 1a, the distribution of the ECC and satellite profiles is consistent above the 50 hPa level, and the satellite data between 300 and 50 hPa shows a substantial increase. The ECC and AIRS profiles are more consistent below 300 hPa. As shown in Fig. 1b, in the UTLS, the ozone values of MLS and AIRS are generally larger than those of ECC and the relative deviation of AIRS near 100 hPa (tropopause) is greater than MLS.

In order to calculate the ozone effective temperature, it is necessary to verify the satellite temperature profile. According to the comparison of ozone profiles, Fig. 2 shows the comparison and deviation between the MLS and AIRS temperature products and iMet temperature profile on March 5, 2014. Fig. 2a shows that the vertical variation of the two satellite temperature profiles is basically consistent with that of the iMet sounding temperature profile, although there is still some deviation. As shown in Fig. 2b, the deviation between the satellite and sounding data is within ±5 °C. The oscillation of MLS deviation in the vertical is more obvious than AIRS. In the troposphere, a negative deviation of MLS and AIRS is observed, and the temperature is low. In the stratosphere, the MLS has a distinct alternation of positive and negative deviations, whereas AIRS has positive deviations.

3.2. Total deviation analysis

3.2.1. Ozone profile deviation

Fig. 3 shows the overall difference distributions of ECC, MLS and AIRS ozone profiles. As shown in Fig. 3a, MLS is close to ECC above 50 hPa and has small dispersion. Under 50 hPa, except at 100 hPa, MLS is generally greater than ECC, and the deviation and dispersion is greatly increased. At 100 hPa, although the relative deviation of MLS and ECC is near zero, the precision is low and the dispersion is large. In addition, the relative deviation at 82.5 hPa is (80.5 ± 65.1) %, which reflects the poor accuracy of the MLS version 4.2 product in the area. This is also reflected in the MLS version 3.3 product (Yan et al., 2015). The obvious oscillations of the relative deviation of AIRS and ECC ozone profiles are shown in Fig. 3b. The relative deviation is small when atmospheric pressure is ≥50 hPa and ≤250 hPa. The average value is <20% and the standard deviation is small, indicating that AIRS products have better quality in the region. Between 200 and 70 hPa near the tropopause, AIRS errors increase substantially and the relative and standard deviation are both large, AIRS is generally greater than ECC. This may be because of the unique location of Kunming, which is on the southeastern Qinghai-Tibet Plateau. Here is an important material exchange channel between the troposphere and stratosphere. At the same time, there was a strong vertical variation of UTLS height and low concentration of ozone at Kunming. AIRS satellite observations with the vertical resolution of the UTLS cannot reveal the actual change of atmospheric ozone like sounding data.

Comparing Fig. 3a and b, the average relative deviation of AIRS in the UTLS region is greater than that of MLS. The relative deviations of AIRS from ECC at 70 and 100 hPa are respectively (105.6 ± 74.9) % and (107.0 ± 67.8) %. As seen, in the UTLS region, the quality of the AIRS product is poorer than that of the MLS product, and they both have limitations. The accuracy of the initial ozone profile is important to the satellite product inversion in the low-latitude plateau region. For example, the initial profile in MLS product inversion comes from operational reanalysis data. These are Global Modeling and Assimilation Office (GMAO) or National Centers for Environmental Prediction (NCEP) data, rather than vertical profiles distributed along latitude or monthly averages (Ahmad et al., 2006). Whether the difference between the initial ozone profile and average of the actual sounding survey will have a meaningful impact on the accuracy of satellite profile products needs further study.

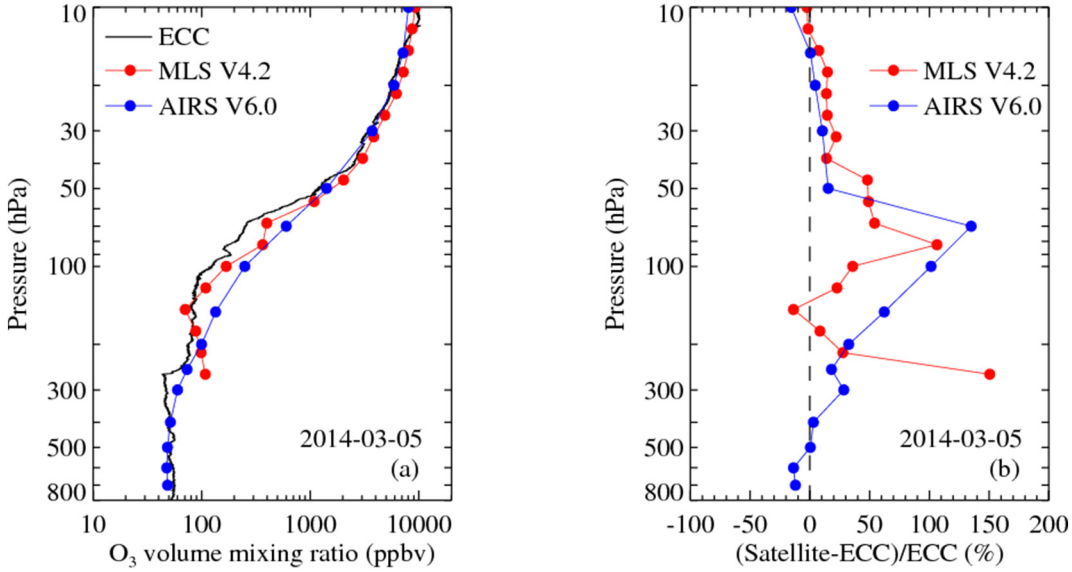

Fig. 1. (a) Comparison between MLS, AIRS and ECC ozone profiles; (b) relative deviation between MLS and ECC and AIRS and ECC over Kunming on March 5, 2014.

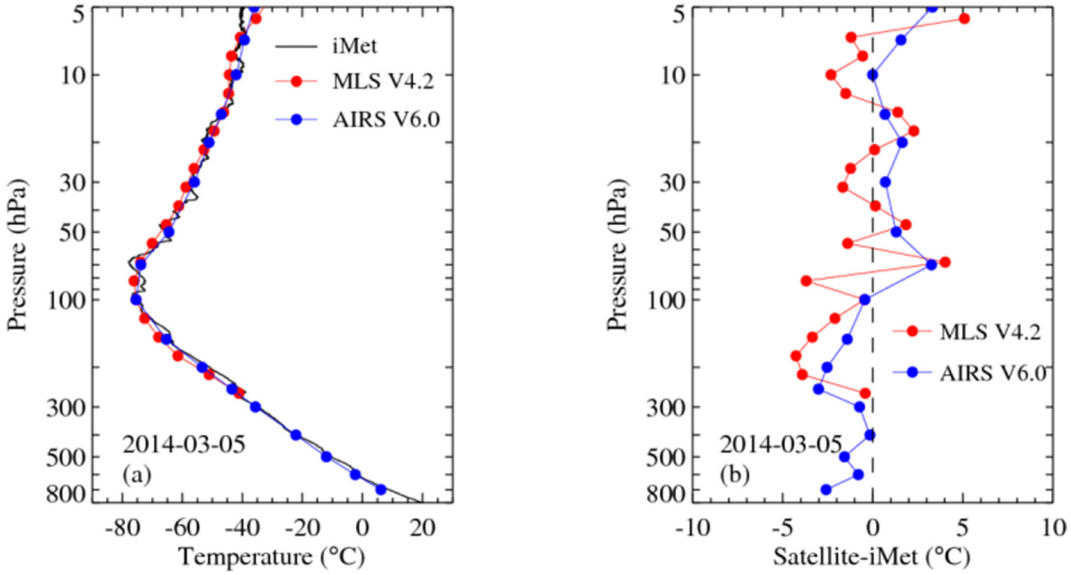

Fig. 2. (a) Comparison between MLS, AIRS and iMet temperature profiles; (b) deviation between MLS and iMet and AIRS and iMet over Kunming on March 5, 2014.

To obtain more detailed information, a comparison of relative deviations in spring (MAM), summer (JJA), autumn (SON) and winter (DJF) are shown Fig. 4, with about nine samples per season. For the relative deviation between MLS and ECC, the distribution above 50 hPa is similar to the overall difference distributions in the four seasons, with the relative deviation between −20% and 20%. In spring, the relative deviation of MLS is 29–68% larger than ECC below 50 hPa, and the standard deviation is greater than in other seasons; the dispersion is substantial. The relative deviation distributions of summer and autumn were similar, and the accuracy is slightly greater than those of winter and spring. However, the relative deviation at 82.5 hPa is still large, even reaching 125% in autumn. In winter, MLS is 17–55% larger than ECC below 50 hPa, and the standard deviation is slightly less than in spring. Compared with MLS, the distribution of AIRS relative deviation is consistent across the four seasons and is similar to the overall difference distribution, but it is substantially larger (33–133%) than the ECC between 150 and 70 hPa.

It has been noted that there is a great deviation between 150 and 70 hPa in the AIRS version 6 ozone product over Kunming, with an average maximum of 60–110%. However, it is found during the validation of the ozone profile product of AIRS version 4 over Beijing that the deviation between the ozone profile product and sounding profile is within 10% in the UTLS (400–70 hPa) region (Bian et al., 2007). Because Kunming is a typical low-latitude plateau monsoon climate area, the vertical distribution of ozone is much different from that of other regions in China (Zheng et al., 2005), and seasonal variation of the ozone profile is also different from that of other latitudes. After establishment of the summer monsoon, a regional "low ozone value" phenomenon may occur over the Qinghai-Tibet Plateau and surrounding areas (Zhou et al., 1995). AIRS data are not sensitive enough to show a large deviation around the tropopause in the Kunming area and cannot reflect actual ozone evolution. In general, ozone concentrations of satellite ozone products near the tropopause of the low-latitude plateau are higher than those observed by ECC sounding.

3.2.2. Temperature profile deviation

Fig. 5 shows overall distributions of all iMet sounding temperatures and MLS and AIRS temperature profile deviations. As shown in Fig. 5a,

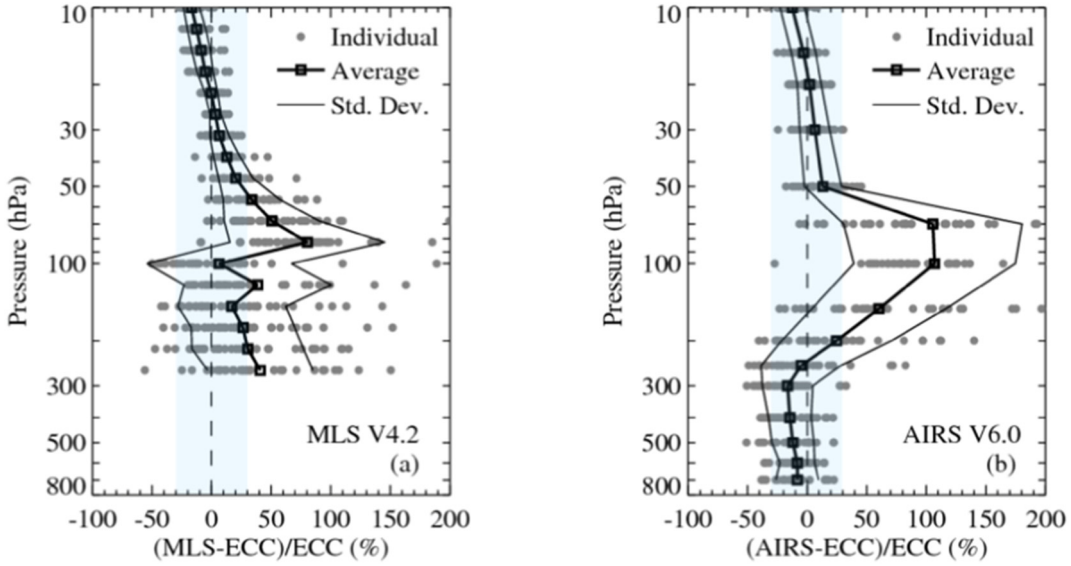

Fig. 3. Overall distribution of relative deviation of ozone profiles between MLS and ECC and AIRS and ECC.

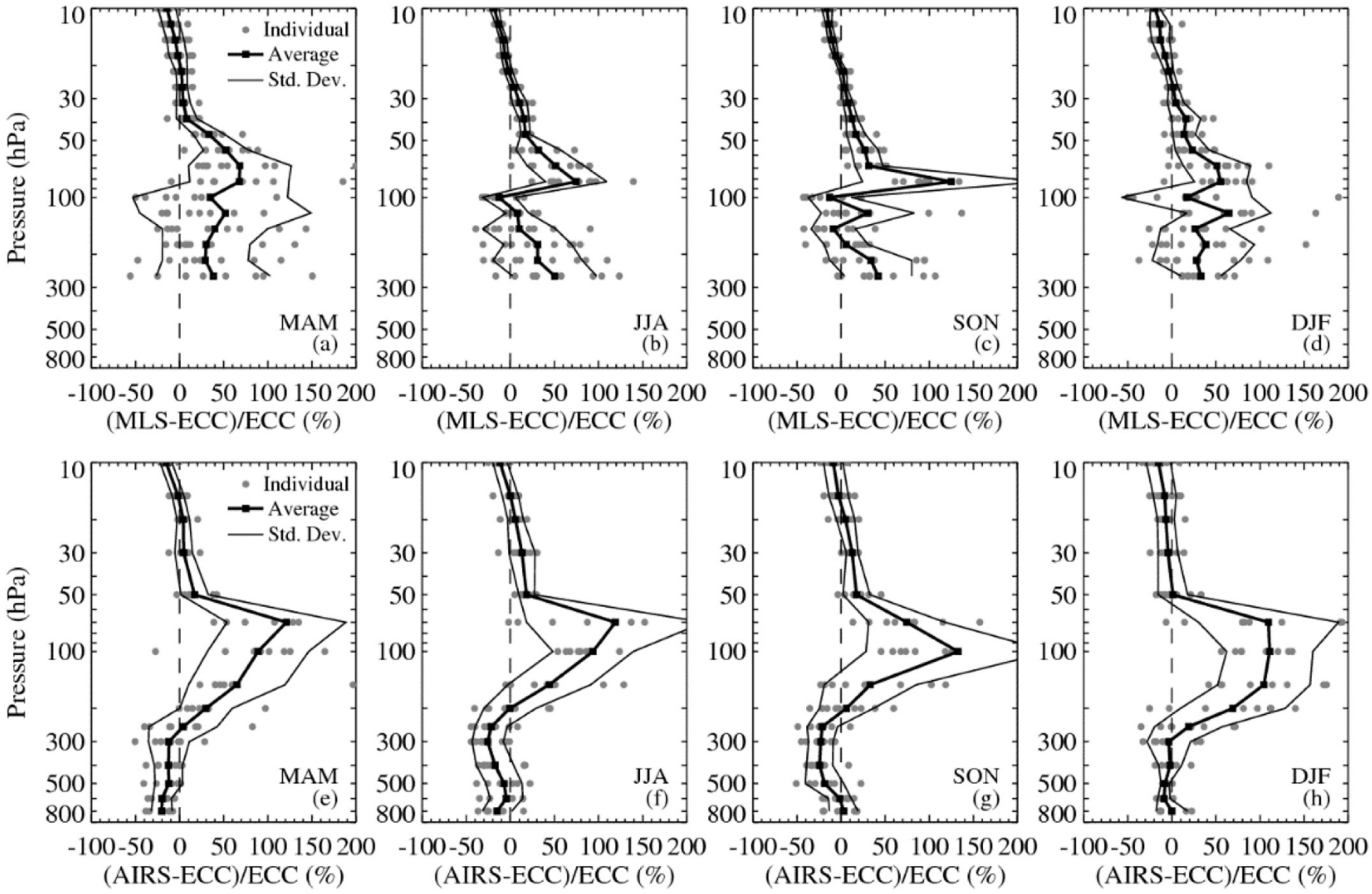

Fig. 4. Seasonal distribution of relative deviation of ozone profiles between MLS and ECC and AIRS and ECC.

the average temperature deviation of MLS shows "positive–negative–positive–negative" oscillation tendency from top to bottom. MLS is greater than iMet by 1–3 °C between 5.6 and 17.8 hPa, and is more scattered. Between 21.5 and 82.5 hPa, the deviation of MLS shows oscillation and the standard deviation is low. From 100 to 261 hPa in the upper troposphere, the MLS temperature is low by 1–4 °C and has an increased standard deviation. As shown in Fig. 5b, the average temperature deviation of AIRS shows a "positive–negative" oscillation tendency from top to bottom. In the stratosphere between 5 and 70 hPa, AIRS is 0–3 °C greater than iMet and the standard deviation is greater than that in the troposphere. The temperature deviation of AIRS between 100 and 700 hPa in the troposphere is slightly larger than that of iMet at 600 hPa and lower by 1–2 °C in other pressure layers, and the standard deviation is decreasing. It is seen that the

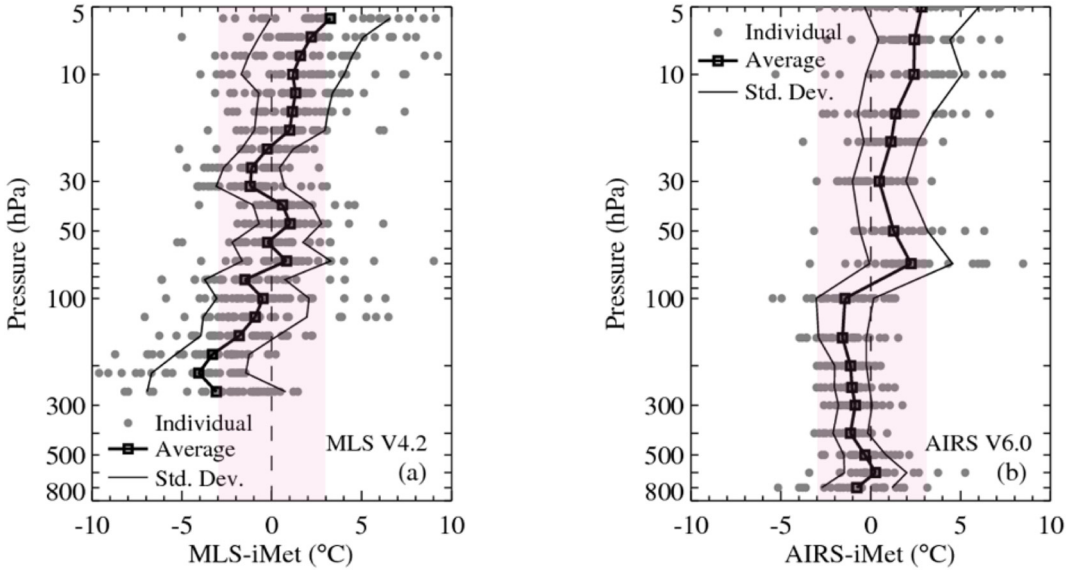

Fig. 5. Overall distribution of deviation of temperature profiles between MLS and iMet and AIRS and iMet.

accuracy of AIRS temperature products in the troposphere is slightly greater than that of MLS.

Fig. 6 shows the deviation of temperature profiles between MLS and iMet and AIRS and iMet in different seasons. It is evident that the seasonal distribution of MLS deviation is similar to the overall distribution characteristics, and the "positive–negative–positive–negative" oscillation is evident. The deviation and dispersion in spring and summer are greater than those in autumn and winter, especially in the troposphere. Between 177.8 and 261.0 hPa in spring and summer, the MLS temperature is 5–6 °C lower than iMet. The standard deviation is substantially greater than those in autumn and winter. This indicates that the quality of the MLS temperature product in the troposphere is slightly inferior in spring and summer. It is also seen that the AIRS deviation for the four seasons basically follows the "positive–negative" vertical distribution. However, the temperature at 600 and 700 hPa in autumn and 700 hPa in winter is slightly warmer.

3.3. Correlation of ozone/temperature

3.3.1. Correlation of ozone

In different pressure layers, the MLS and AIRS were analyzed by linear regression ($O_{3\ (MLS,AIRS)} = \alpha + \beta O_{3(ECC)}$) with the ECC detection results. ECC system error was ignored here. The ECC data are accurate and the random error is assumed to be consistent throughout the atmosphere. The intercept α partly reflects the absolute error of the MLS and AIRS system. The physical meaning of slope β is the sensitivity of MLS and AIRS, which is linear.

Fig. 7 shows the correlation between MLS and ECC in different pressure layers. In the upper troposphere, the linear relationship between MLS and ECC is strong, but slightly reduced at 100 hPa. In the stratosphere, with the increase of height, the linear relationship had a tendency to decrease. At 31.6 hPa, the linear relationship is less obvious. Accordingly, the correlation of AIRS and ECC is shown in Fig. 8. In the troposphere below 200 hPa, the linear relationship between AIRS and ECC is not clear but increases slightly in the stratosphere.

According to Table 2, the range of slope β of MLS and AIRS is 0.33–0.93 and 0.16–0.88, respectively. The sensitivity of MLS in the stratosphere between 20 and 10 hPa is weaker than AIRS, but generally stronger at other levels. The sensitivity of the MLS version 4.2 ozone product in the troposphere is greatly improved over that of version 3.3, and the corresponding $\alpha/\overline{O}_{ECC}$ is also reduced. Between 100.0 and 261.0 hPa for version 4.2 and 3.3 products, the mean β is 0.75 (all pass the significance test) and 0.52, and the mean $\alpha/\overline{O}_{ECC}$ values are 45.9% and 65.5% (linear fit of MLS version 3.3; ECC is based on Table 3 in Yan et al., 2015). AIRS ozone products have weak sensitivity in the troposphere and lower stratosphere. Between 70 and 700 hPa, the mean β is 0.29, and only 50% pass the significance test. In other words, AIRS ozone products have great uncertainty in reflecting ozone changes in this region. Similarly, although the numerical value of α is small in this range, $\alpha/\overline{O}_{ECC}$ is larger because of the low average ozone concentration, especially near 100 hPa. This also indicates that the remote sensing products of AIRS have large error in the troposphere and stratosphere.

3.3.2. Correlation of temperature

From the sensitivity analysis of ozone products, Fig. 9 shows the correlation of MLS and iMet temperature products in various pressure layers. As seen, in addition to weak sensitivity at 31.6 and 46.4 hPa, the linear relationship between MLS temperature products and iMet temperature at other levels is strong. In particular, the values of β at 21.5 and 100 hPa are near 1.0 and the sensitivity is very strong. Similarly, Fig. 10 shows the correlation of AIRS and iMet temperatures in

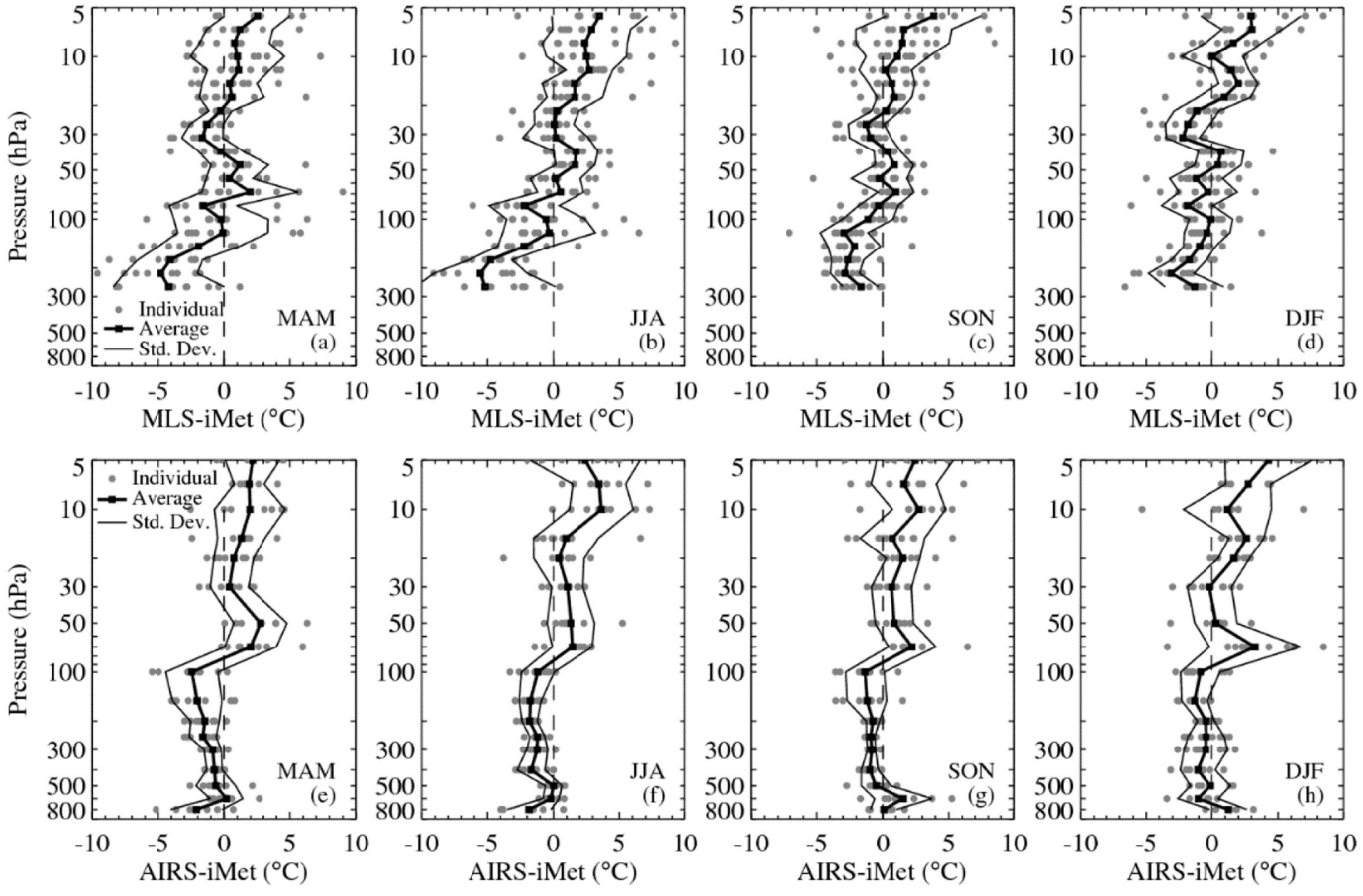

Fig. 6. Seasonal distribution of relative deviation of temperature profiles between MLS and iMet and AIRS and iMet.

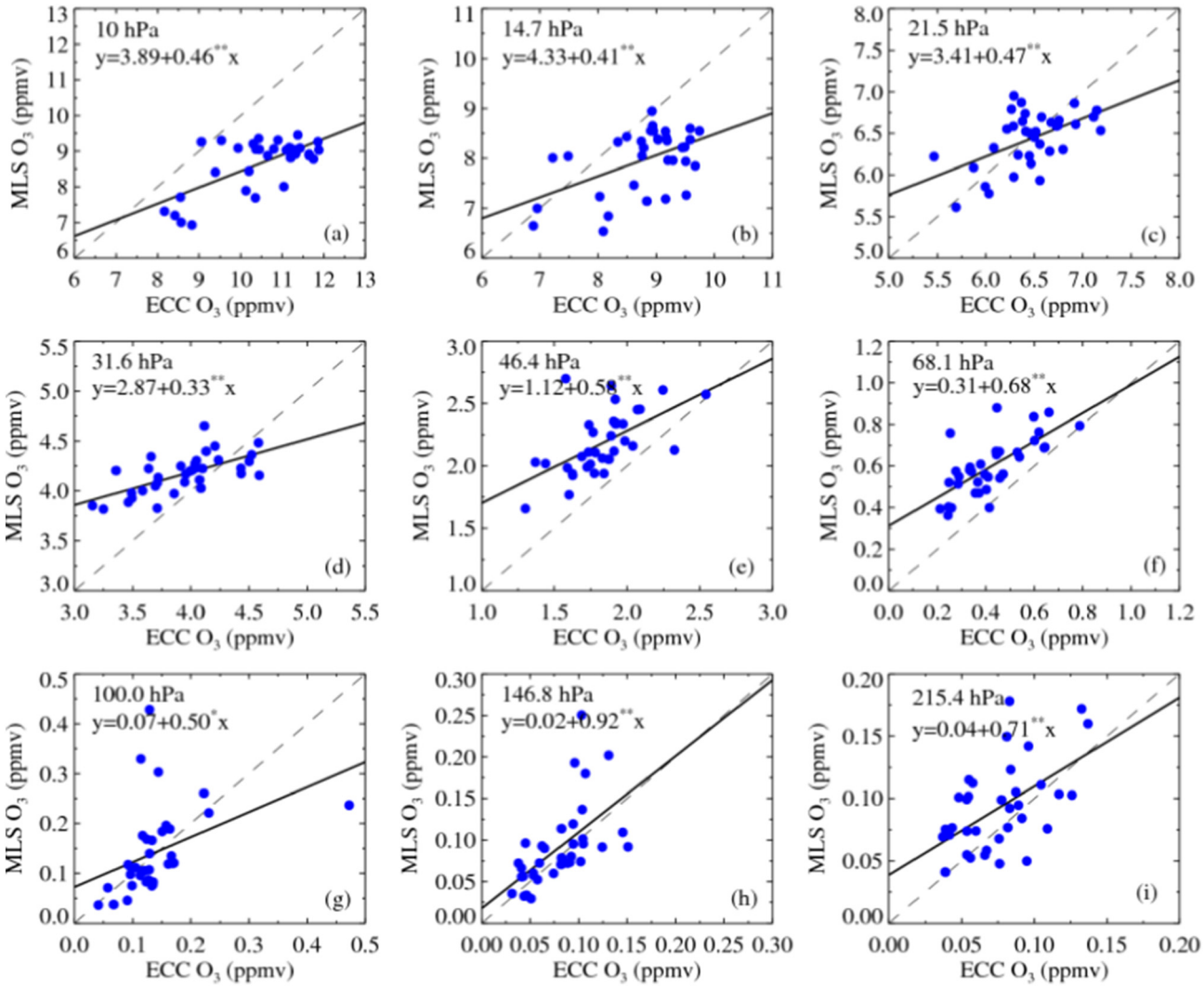

Fig. 7. Correlation of MLS and ECC in different pressure layers (* or ** represents $p < 0.05$ or 0.01, respectively).

different atmospheric layers. It is seen that the sensitivity is slightly less at 30 and 50 hPa, and the linear relationship between the AIRS temperature product and iMet temperature is stronger in other layers. Obviously, the temperature products of MLS and AIRS have similar sensitivities.

Table 3 shows that the ranges of slope β of MLS and AIRS are 0.31–1.07 and 0.38–0.98, respectively, and all pass the significance test. The sensitivity of MLS at 31.6–56.2 hPa is less and the corresponding $\alpha/\overline{T}$iMet(%) is larger. This indicates that the MLS temperature product is still uncertain in its indication of temperature change in this region. Similarly, from 30 to 50 hPa, although the sensitivity of AIRS is slightly greater than that of MLS, it is still a low-value layer relative to other pressure layers. In general, the sensitivity of AIRS temperature products is greater in the troposphere than stratosphere. Especially in the upper troposphere, AIRS is more accurate in the inversion of the temperature distribution.

4. Effective height and effective temperature of ozone

First, according to the sounding experiment, it is necessary to use satellite data to supplement missing data above the detection altitude so that the height of the ozone and temperature profiles can reach the top of the stratosphere. For this purpose, the sounding profiles were spliced with the ozone and temperature profiles of MLS and AIRS and labeled ECC_MLS and ECC_AIRS. At the same time, the ozone profiles (temperature profile) of MLS, AIRS, ECC, ECC_MLS and ECC_AIRS were used to calculate H_{eff} and T_{eff} for comparison and analysis.

4.1. Effective height

Fig. 11 shows the monthly variation of five H_{eff} calculated using five monthly average ozone profiles. The H_{eff} of each month and the annual average are listed in Table 4. As seen, the five annual average H_{eff} are 26.72, 25.60, 21.81, 24.99 and 24.99 km. Among these, $H_{eff(MLS)}$ is the highest, $H_{eff(ECC)}$ is the lowest, and $H_{eff(ECC\_MLS)}$ and $H_{eff(ECC\_AIRS)}$ are nearly indistinguishable and close to $H_{eff(AIRS)}$. Differences are caused by different data structures of the five ozone profiles. The H_{eff} calculated using ECC data to which was added "high-altitude" satellite data is considered to be "true value". The $H_{eff(MLS)}$ is higher than the other H_{eff} because of the lack of "low-altitude" data of MLS from the surface to mid-troposphere. The $H_{eff(ECC)}$ is the lowest and under the true value about 3.2 km, because of the lack of high-altitude data of ECC above 10 hPa. AIRS contains data from the surface to upper air, so $H_{eff(AIRS)}$ is nearest the true value. However, because the poor vertical resolution, there is a difference between the $H_{eff(AIRS)}$ and true value. Therefore, it is shown that when the high-resolution sounding data are used to

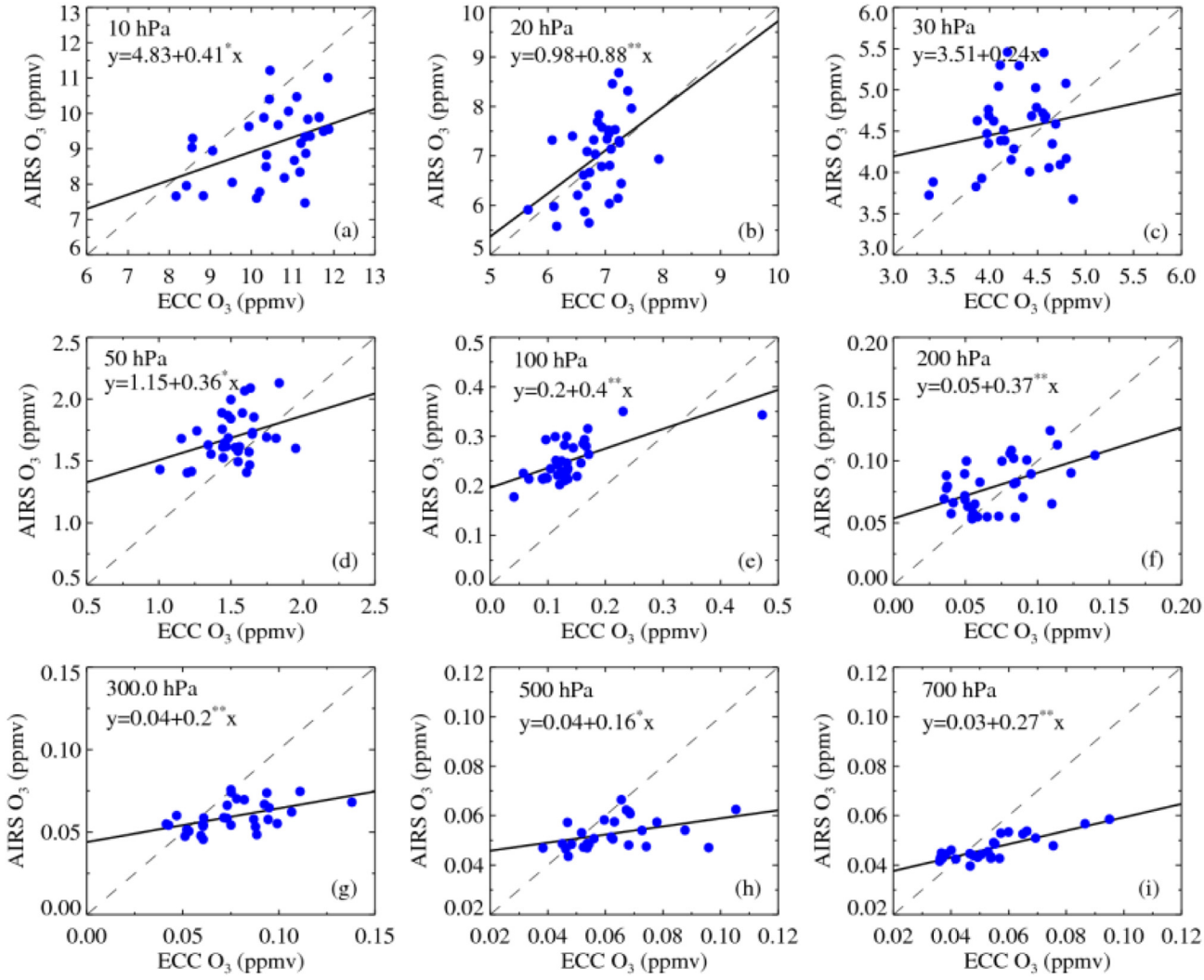

Fig. 8. Correlation of AIRS and ECC in different pressure layers (* or ** represents $p < 0.05$ or 0.01, respectively).

calculate the H_{eff} of ozone, it causes error that cannot be ignored because of the lack of high-altitude data. Thus, it is necessary to use the method of splicing high-altitude satellite data to effectively reduce the error.

From Table 4, it is seen that the H_{eff} of ECC_MLS and ECC_AIRS have little difference; both are between 24.36 and 25.51 km, with an average of 24.99 km. They are slightly higher in summer and autumn than in

Table 2
Linear coefficients of fit of MLS and AIRS with ECC ozone observed values (* or ** represents $p < 0.05$ or 0.01, respectively).

Pressure (hPa)	MLS V4.2					Pressure (hPa)	AIRS V6.0				
	α	β	$\alpha/\overline{O}$ECC (%)	$\overline{O}$ECC (ppmv)	Sample		α	β	$\alpha/\overline{O}$ECC (%)	$\overline{O}$ECC (ppmv)	Sample
10.0	3.89	0.46**	37.1	10.465	33	10	4.83	0.41**	46.0	10.498	32
12.1	3.76	0.47**	39.4	9.541	34	15	3.40	0.57**	39.4	8.631	33
14.7	4.33	0.41**	49.2	8.798	34	20	0.98	0.88**	14.3	6.879	34
17.8	4.09	0.41**	53.6	7.638	34	30	3.51	0.24	82.2	4.274	34
21.5	3.41	0.47**	52.8	6.455	35	50	1.15	0.36*	76.2	1.511	34
26.1	3.09	0.43**	59.8	5.164	35	70	0.60	0.20	160.2	0.376	35
31.6	2.87	0.33**	72.9	3.936	35	100	0.20	0.40**	144.8	0.135	35
38.3	1.96	0.43**	69.4	2.823	35	150	0.07	0.59**	86.8	0.077	34
46.4	1.12	0.58**	61.4	1.832	35	200	0.05	0.37**	75.8	0.070	34
56.2	0.95	0.41**	89.2	1.067	35	250	0.05	0.18	70.6	0.074	32
68.1	0.31	0.68**	74.0	0.421	35	300	0.04	0.20	59.7	0.074	31
82.5	0.21	0.69**	94.3	0.218	36	400	0.04	0.19	64.6	0.066	30
100.0	0.07	0.50**	52.3	0.138	36	500	0.04	0.16	69.6	0.061	27
121.2	0.06	0.71**	59.1	0.101	36	600	0.03	0.30*	60.1	0.054	27
146.8	0.02	0.92**	22.4	0.080	36	700	0.03	0.27*	61.8	0.052	27
177.8	0.02	0.93**	29.0	0.074	36	–	–	–	–	–	–
215.4	0.04	0.71**	51.7	0.075	36	–	–	–	–	–	–
261.0	0.05	0.73**	61.0	0.075	36	–	–	–	–	–	–

Table 3
Linear fitting coefficients of MLS and AIRS with iMet temperature observed values (* or ** represents $p < 0.05$ or 0.01, respectively).

Pressure (hPa)	MLS V4.2					Pressure (hPa)	AIRS V6.0				
	α	β	$\alpha/\overline{T}$iMet (%)	$\overline{T}$iMet (°C)	Sample		α	β	$\alpha/\overline{T}$iMet (%)	$\overline{T}$iMet (°C)	Sample
5.6	−16.2	0.51**	41.2	−39.2	32	5	−13.9	0.56**	36.1	−38.4	32
6.8	−10.2	0.70**	24.5	−41.5	32	7	−5.1	0.82**	12	−42.2	32
8.3	−16.1	0.60**	36.6	−44	32	10	−15.3	0.61**	33.5	−45.6	32
10.0	−18.3	0.57**	40.3	−45.5	33	15	−19.5	0.57**	39.8	−49.1	33
12.1	−1.5	0.94**	3.1	−47.5	34	20	−16.1	0.67**	31	−52	34
14.7	−10.3	0.77**	21.1	−49	34	30	−26.8	0.51**	48.1	−55.8	34
17.8	−3.9	0.90**	7.6	−50.9	34	50	−39.8	0.38**	60.3	−65.9	34
21.5	0.4	1.01**	−0.8	−52.3	35	70	−32.7	0.55**	42.6	−76.8	35
26.1	−18.3	0.68**	33.7	−54.3	35	100	−18.2	0.78**	24	−75.9	35
31.6	−38.9	0.33**	68.7	−56.5	35	150	−25.0	0.63**	39.3	−63.5	34
38.3	−41.0	0.31*	68	−60.2	35	200	−9.0	0.84**	18	−50.4	34
46.4	−41.6	0.34**	64.8	−64.2	35	250	−4.2	0.92**	10.7	−39.1	32
56.2	−35.7	0.48**	51.9	−68.7	35	300	−4.5	0.88**	14.8	−30.2	31
68.1	−29.6	0.60**	38.9	−76	35	400	−3.0	0.88**	19.4	−15.6	30
82.5	−16.8	0.80**	21.7	−77.5	36	500	−0.4	0.98**	7.5	−5.5	27
100.0	4.9	1.07**	−6.4	−75.7	36	600	0.9	0.74**	56.7	1.6	27
121.2	−12.9	0.83**	18.3	−70.6	36	700	2.8	0.66**	30.1	9.2	27
146.8	−20.7	0.71**	32.2	−64.3	36	–	–	–	–	–	–
177.8	−29.4	0.54**	52.4	−56	36	–	–	–	–	–	–
215.4	−20.0	0.66**	42.9	−46.7	36	–	–	–	–	–	–
261.0	−14.4	0.70**	38.6	−37.3	36	–	–	–	–	–	–

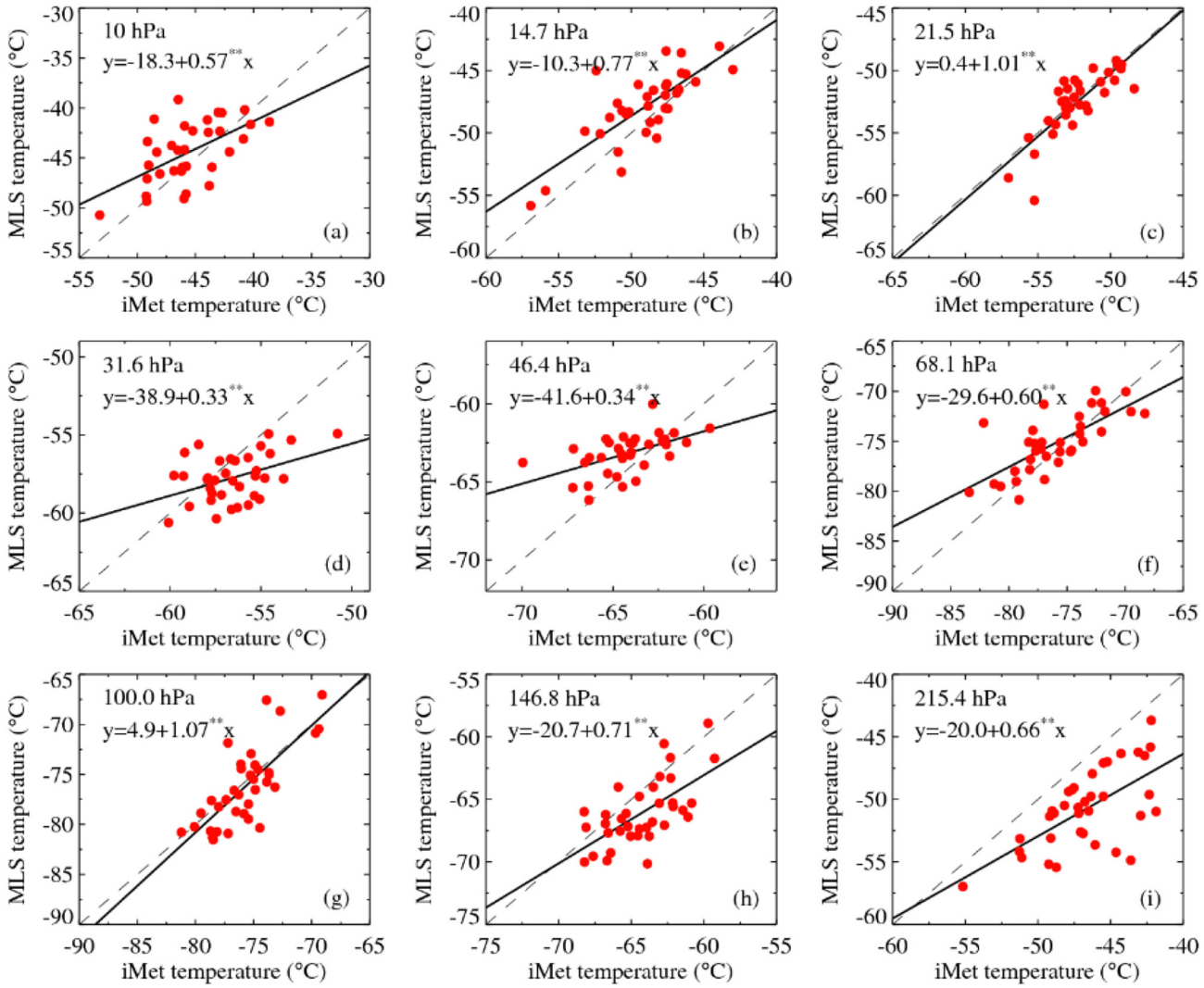

Fig. 9. Correlation of temperature of MLS and iMet in different pressure layers (* or ** represents $p < 0.05$ or 0.01, respectively).

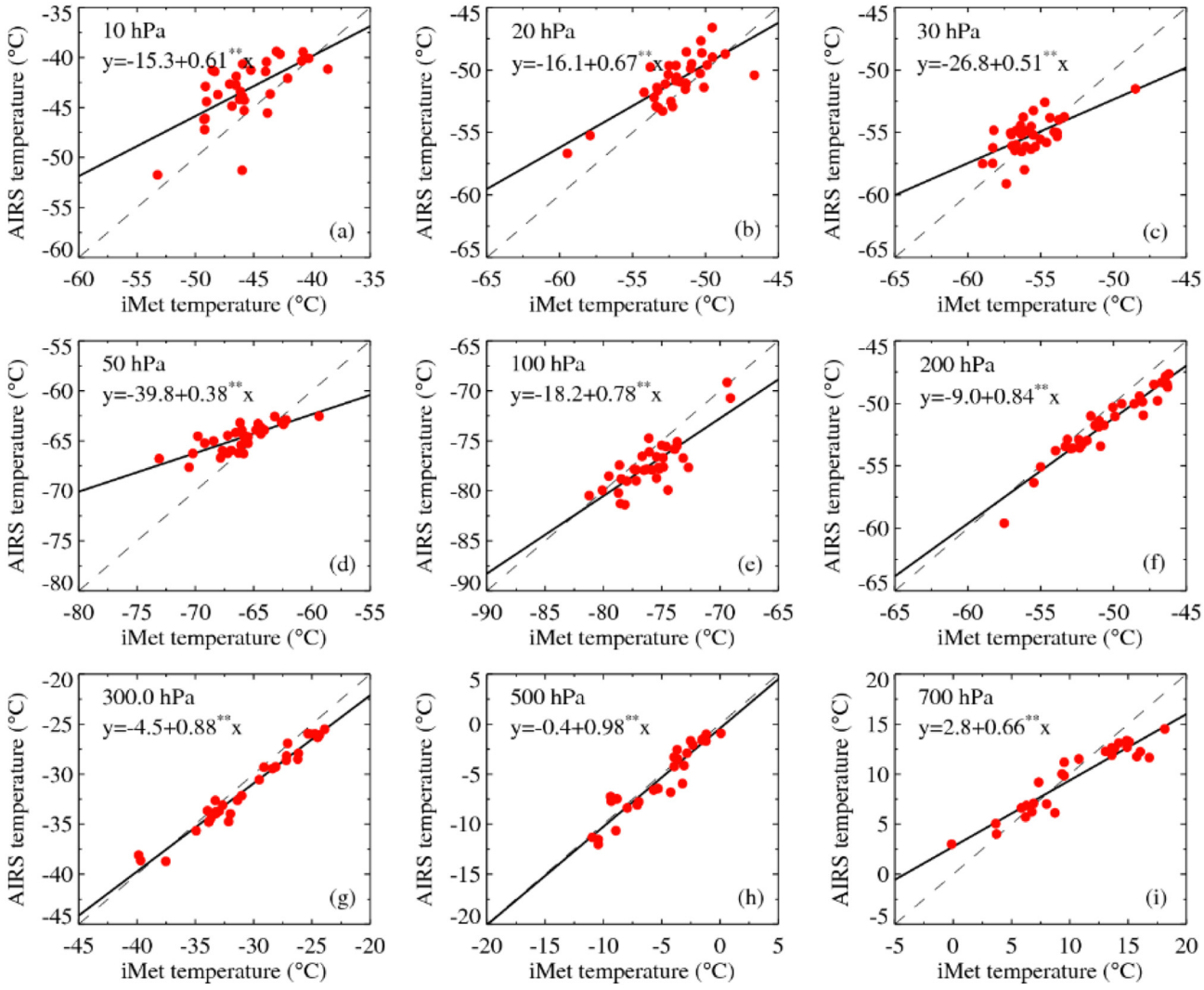

Fig. 10. Correlation of temperature of AIRS and iMet in different pressure layers (* or ** represents $p < 0.05$ or 0.01, respectively).

winter and spring. Obviously, the operational H_{eff} used by the Kunming ozone observation station is 23.0 km, which is not consistent with the actual ozone layer height at the station and must be revised on a monthly or seasonal basis.

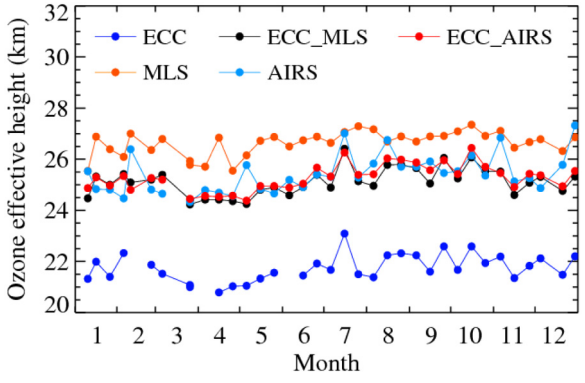

Fig. 11. Monthly variation of five effective height datasets calculated using five ozone profile datasets from Kunming.

4.2. Effective temperature

Fig. 12 shows the monthly variation of five T_{eff} calculated using five monthly average temperature profiles and corresponding ozone profile data. Similarly, the T_{eff} of each month and annual average are listed in Table 4. It is seen that the annual average T_{eff} are 51.3, 48.8, 48.8, 45.5 and 45.6 °C. Among these, $T_{eff(MLS)}$ is the lowest, $T_{eff(AIRS)}$ and $T_{eff(ECC)}$ are similar, and $T_{eff(ECC\_MLS)}$ and $T_{eff(ECC\_AIRS)}$ are the highest. The reason for the difference of T_{eff} calculated using different profiles is analogous to that of H_{eff}. Because of the lack of "low-altitude" temperature and ozone data, the $T_{eff(MLS)}$ is low. For AIRS and ECC, owing to defects in the data, the $T_{eff(AIRS)}$ and $T_{eff(ECC)}$ are lower than the true value of ~3.2 °C. Therefore, when calculating the T_{eff} of ozone, the sounding data were spliced with the satellite data to effectively reduce the error.

The T_{eff} of ECC_MLS and ECC_AIRS vary from −48.3 to −43.5 °C, with averages −45.5 and −45.6 °C, respectively. They were slightly larger in spring and summer than in autumn and winter. The operational T_{eff} used by the Dobson (D003) and Brewer (B198) spectrometer at Kunming station are −46.3 and −45 °C, respectively, which do not reflect the actual inter-monthly variation of temperature and must be corrected according to seasonal changes. At present, the empirical standard ozone effective temperature values of the Dobson (D003) and Brewer (B198) spectrometers at Kunming Station are −46.3 and −45

Table 4
Comparison of monthly means of ozone effective height and effective temperature calculated using five sets of ozone and temperature profiles over Kunming.

Month	H_{eff} (km)					T_{eff} (°C)				
	MLS	AIRS	ECC	ECC_MLS	ECC_AIRS	MLS	AIRS	ECC	ECC_MLS	ECC_AIRS
1	26.38	25.25	21.59	24.76	24.69	−53.5	−51.2	−51.4	−48.2	−48.3
2	26.55	25.40	22.11	25.08	24.82	−53.4	−51.2	−51.4	−47.6	−47.9
3	26.28	24.71	21.23	24.52	24.44	−52.5	−49.6	−49.8	−46.5	−46.5
4	26.15	24.90	21.26	24.40	24.36	−51.4	−47.5	−45.7	−43.5	−43.6
5	26.66	25.27	21.72	24.84	24.76	−50.5	−48.3	−47.3	−43.9	−44.0
6	26.83	25.36	21.70	24.86	25.01	−49.7	−46.9	−47.4	−43.9	−43.7
7	27.08	26.01	22.09	25.37	25.31	−50.3	−48.4	−48.4	−45.2	−45.3
8	27.02	26.24	21.98	25.34	25.45	−50.3	−48.1	−48.1	−45.0	−44.9
9	26.95	25.86	22.14	25.41	25.43	−51.4	−48.6	−49.2	−46.2	−46.3
10	27.22	25.85	22.07	25.45	25.51	−51.2	−48.5	−48.2	−45.6	−45.6
11	26.83	25.89	21.81	24.90	24.93	−50.7	−49.1	−49.1	−45.6	−45.7
12	26.73	26.16	21.93	24.96	24.95	−50.4	−48.0	−48.8	−45.4	−45.3
Avg.	26.72	25.60	21.81	24.99	24.99	−51.3	−48.8	−48.8	−45.5	−45.6

°C, respectively, which do not reflect the actual inter-monthly variation of temperature and must be corrected according to seasonal changes. In the preliminary calculation and analysis of the improvement of total ozone observation data, we only considered the inter-monthly variation of effective temperature. When their effective temperature is −48.3 °C (Table 4), it produces deviation between the observed data of diurnal variation in total ozone and observed data using the empirical standard ozone effective temperature values of the diurnal variation in total ozone during January from the two instruments, with average deviation ~1.2%. We also found that Dobson is more dependent on the effective temperature than Brewer. Moreover, because of the large seasonal fluctuation of total ozone, the sensitivity of total ozone change to effective temperature seasonal variation is different, and total ozone change in autumn and winter is greater than that in spring and summer.

5. Conclusions

In this work, verification and analysis were done for the satellite ozone and temperature profile products of Aura-MLS version 4.2 and Aqua-AIRS version 6.0 in the low-latitude plateau region, based on data of the sounding experiment. The ozone H_{eff} and T_{eff} were calculated using different schemes composed by satellite and sounding data. The following conclusions were drawn.

In the UTLS region, the vertical distribution of the ozone differences of MLS and AIRS has significant oscillation and scatter, and MLS and AIRS data are generally larger than ECC detection values. MLS has the maximum deviation at 82.5 hPa, with an average of (80.5 ± 65.1) %, whereas at the other levels this is within 50%. The sensitivity of the MLS version 4.2 ozone product in the troposphere is greatly improved over that of version 3.3, and their mean β values between 100.0 and 261.0 hPa are 0.75 (all pass the significance test) and 0.52, respectively.

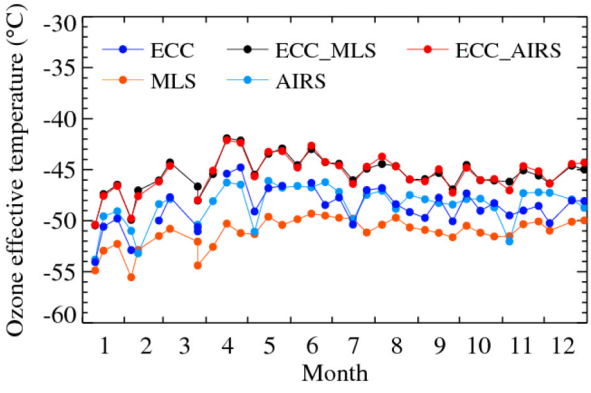

Fig. 12. Monthly variation of five effective temperature datasets calculated using five temperature profile and corresponding ozone profile datasets from Kunming.

The relative deviations of AIRS from ECC at 70 and 100 hPa are (105.6 ± 74.9) % and (107.0 ± 67.8) %. AIRS ozone products have weak sensitivity in the troposphere and lower stratosphere. Between 70 and 700 hPa, the mean β is 0.29 and only 50% pass the significance test. The accuracy of MLS is slightly greater in summer and autumn than in winter and spring. The seasonal variation of AIRS deviation is not great. In general, in the UTLS region, the quality of the AIRS product is poorer than that of the MLS product, and both have limitations.

The deviation of MLS and AIRS temperature products is in the range of ±3 °C. Above 17.8 hPa, MLS values are on the high side by 1–3 °C. Below 100 hPa, MLS is low by 1–4 °C. Above 70 hPa, AIRS is high by 0–3 °C. Below 100 hPa, AIRS is low by 1–2 °C. The quality of the MLS temperature product in the troposphere is slightly inferior in spring and summer with underestimates of 5–6 °C, and seasonal variation of the difference of the AIRS temperature product is not obvious. In general, both MLS and AIRS temperature products have great sensitivity and could capture the vertical distribution and variation of temperature.

The sounding data have high resolution but miss the high-altitude part. When these data were used to calculate the H_{eff} and T_{eff}, it led to large errors of 3.2 km and 3.3 °C, respectively. Therefore, the sounding data must be spliced with the satellite data to effectively reduce the error. The profiles from the merger of MLS and AIRS data, whose calculated values show little difference, could be used complementarily. The H_{eff} at Kunming is between 24.36 and 25.51 km with an average of 24.99 km. T_{eff} is between −48.3 and −43.5 °C with an average of −45.5 °C. Therefore, the operative standard parameters ($H_{eff(0)}$ = 23 km, $T_{eff(0)}$ = −46.3 °C (or −45 °C)) do not conform to our data and must be corrected.

Acknowledgments

This study was supported by the National Natural Science Foundation of China under grants 41807308, 21777026, 41641044, 21477021 and 41275045. Thanks go to NASA's GES DISC for satellite ozone and temperature profile products.

References

Ahmad, S.P., Waters, J., Johnson, J., Gerasimov, I., Leptoukh, G., Kempler, S., 2006. Atmospheric composition data products from the eos aura mls. Ams Annual Meeting.

Bernhard, G., Evans, R.D., Labow, G.J., Oltmans, S.J., 2005. Bias in Dobson total ozone measurements at high latitudes due to approximations in calculations of ozone absorption coefficients and air mass. J. Geophys. Res. 110, D10305. https://doi.org/10.1029/2004JD005559.

Berthet, G., Renard, J.-B., Ghysels, M., Durry, G., Gaubicher, B., Amarouche, N., 2013. Balloon-borne observations of mid-latitude stratospheric water vapour: comparisons with HALOE and MLS satellite data. J. Atmos. Chem. 70 (3), 197–219.

Bhartia, P.K., Silberstein, D., Monosmith, B., Fleig, A.J., 1985. Standard profiles of ozone from ground to 60 km obtained by combining satellites and ground based measurements. In: Zerefos, C.S., Ghazi, A. (Eds.), Atmospheric Ozone: Proceeding of the Quadrennial Ozone Symposium Held in Halkidiki, Greece, 3–7 September 1984. Springer, New York, pp. 243–247.

Bian, J., Gettelman, A., Chen, H., Pan, L.L., 2007. Validation of satellite ozone profile retrievals using Beijing ozonesonde data. J. Geophys. Res. 112, D06305. https://doi.org/10.1029/2006JD007502.

Bodeker, G.E., Boyd, I.S., Matthews, W.A., 1998. Trends and variability in vertical ozone and temperature profiles measured by ozonesondes at Lauder, New Zealand: 1986–1996. J. Geophys. Res. 103 (D22), 28661–28681.

Borchi, F., Pommereau, J.P., Garnier, A., Pinharanda, M., 2005. Evaluation of SHADOZ sondes, HALOE and SAGE II ozone profiles at the tropics from SAOZ UV-vis remote measurements onboard long duration balloons. Atmos. Chem. Phys. 5, 1381–1397.

Divakarla, M., Barnet, C., Goldberg, M.D., McMillin, L., Maddy, E.S., Wolf, W., Zhou, L., Liu, X., 2006. Validation of Atmospheric Infrared Sounder temperature and water vapor retrievals with matched radiosonde measurements and forecasts. J. Geophys. Res. 111. https://doi.org/10.1029/2005JD006116.

Divakarla, M., Barnet, C., Goldberg, M., Maddy, E., Irion, F., Newchurch, M., Liu, X., Wolf, W., Flynn, L., Labow, G., Xiong, X., Wei, J., Zhou, L., 2008. Evaluation of Atmospheric Infrared Sounder ozone profiles and total ozone retrievals with matched ozonesonde measurements, ECMWF ozone data, and Ozone Monitoring Instrument retrievals. J. Geophys. Res. 113, D15308. https://doi.org/10.1029/2007JD009317.

Dueñas, C., Fernández, M.C., Cañete, S., Carretero, J., Liger, E., 2002. Assessment of ozone variations and meteorological effects in an urban area in the Mediterranean coast. Sci. Total Environ. 299, 97–113. https://doi.org/10.1016/s0048-9697(02)00251-6.

Elminir, H.K., 2005. Dependence of urban air pollutants on meteorology. Sci. Total Environ. 350, 225–237. https://doi.org/10.1016/j.scitotenv.2005.01.043.

Froidevaux, L., Livesey, N.J., Read, W.G., Jiang, Y.B., Jimenez, C., Filipiak, M.J., 2006. Early validation analyses of atmospheric profiles from EOS MLS on the Aura satellite. IEEE Trans. Geosci. Remote Sens. 44 (5), 1106–1121. https://doi.org/10.1109/TGRS.2006.864366.

Froidevaux, L., Jiang, Y.B., Lambert, A., Livesey, N.J., Read, W.G., Waters, J.W., 2008. Validation of Aura Microwave Limb Sounder stratospheric ozone measurements. J. Geophys. Res. 113, D15S20. https://doi.org/10.1029/2007JD008771.

Gao, W., Tie, X.X., Xu, J.M., Huang, R.J., Mao, X.Q., Zhou, G.Q., Chang, L.Y., 2017. Long-term trend of O_3 in a mega City (Shanghai), China: characteristics, causes, and interactions with precursors. Sci. Total Environ., 425–433 https://doi.org/10.1016/j.scitotenv.2017.06.099.

Jiang, Y.B., Froidevaux, L., Lambert, A., Livesey, N.J., Read, W.G., Waters, J.W., 2007. Validation of Aura Microwave Limb Sounder ozone by ozonesonde and lidar measurements. J. Geophys. Res. 112. https://doi.org/10.1029/2007JD008776.

Kerr, J.B., Fast, H., McElroy, C.T., Oltmans, S.J., Lathrop, J.A., 1994. The 1991 WMO international ozonesonde intercomparison at Vanscoy, Canada. Atmosphere-Ocean 32, 685–716.

Klenk, K.F., Bhartia, P.K., 1983. Standard ozone profiles from balloon and satellite data sets. J. Clim. Appl. Meteorol. 32, 2012–2022.

Komhyr, W.D., Barnes, R.A., Brothers, G.B., Lathrop, J.A., Opperman, D.P., 1995. Electrochemical concentration cell ozonesonde performance evaluation during STOIC 1989. J. Geophys. Res. 100, 9231–9244.

Li, J., Chen, X.S., Wang, Z.F., Du, H.Y., Yang, W.Y., Sun, Y.L., Hu, B., Li, J.J., Wang, W., Wang, T., Fu, P.Q., Huang, H.L., 2018. Radiative and heterogeneous chemical effects of aerosols on ozone and inorganic aerosols over East Asia. Sci. Total Environ., 1327–1342 https://doi.org/10.1016/j.scitotenv.2017.12.041.

Liu, X., Bhartia, P.K., Chance, K., Froidevaux, L., Spurr, R.J.D., Kurosu, T.P., 2010. Validation of Ozone Monitoring Instrument (OMI) ozone profiles and stratospheric ozone columns with Microwave Limb Sounder (MLS) measurements. Atmos. Chem. Phys. 10, 2539–2549.

Livesey, N.J., Read, W.G., Wagner, P.A., Froidevaux, L., Lambert, A., Manney, G.L., 2015. Version 4.2 Level 2 Data Quality and Description Document. JPL D-33509.

Miller, M.B., Fine, R., Pierce, A.M., Gustin, M.S., 2015. Identifying sources of ozone to three rural locations in Nevada, USA, using ancillary gas pollutants, aerosol chemistry, and mercury. Sci. Total Environ., 483–492 https://doi.org/10.1016/j.scitotenv.2015.03.146.

Pittman, J.V., Pan, L.L., Wei, J.C., Irion, F.W., Liu, X., Maddy, E.S., Barnet, C.D., Chance, K., Gao, R.S., 2009. Evaluation of AIRS, IASI, and OMI ozone profile retrievals in the extratropical tropopause region using in situ aircraft measurements. J. Geophys. Res. 114, D24109. https://doi.org/10.1029/2009JD012493.

Redondas, A., Evans, R., Stuebi, R., Köhler, U., Weber, M., 2014. Evaluation of the use of five laboratory-determined ozone absorption cross sections in Brewer and Dobson retrieval algorithms. Atmos. Chem. Phys. 14, 1635–1648. https://doi.org/10.5194/acp-14-1635-2014.

Scarnato, B., Staehelin, J., Peter, T., Gröbner, J., Stübi, R., 2009. Temperature and slant path effects in Dobson and Brewer total ozone measurements. J. Geophys. Res. 114, D24303. https://doi.org/10.1029/2009JD012349.

Schwartz, M.J., Lambert, A., Manney, G.L., Read, W.G., Livesey, N.J., Froidevaux, L., Ao, C.O., Bernath, P.F., Boone, C.D., Cofield, R.E., Daffer, W.H., Drouin, B.J., Fetzer, E.J., Fuller, R.A., Jarnot, R.F.R., Jiang, J.H., Jiang, Y.B., Knosp, B.W., Krüger, K., Li, J.-L.F., Mlynczak, M.G., Pawson, S., Russell III, J.M., Santee, M.L., Snyder, W.V., Stek, P.C., Thurstans, R.P., Tompkins, A.M., Wagner, P.A., Walker, K.A., Waters, J.W., Wu, D.L., 2008. Validation of the Aura Microwave Limb Sounder temperature and geopotential height measurements. J. Geophys. Res. 113, D15S11. https://doi.org/10.1029/2007JD008783.

Shang, B., Feng, Z.Z., Li, P., Yuan, X.Y., Xu, Y.S., Calatayud, V., 2017. Ozone exposure-and flux-based response relationships with photosynthesis, leaf morphology and biomass in two poplar clones. Sci. Total Environ., 185–195 https://doi.org/10.1016/j.scitotenv.2017.06.083.

Smit, H.G.J., Straeter, W., Johnson, B.J., Oltmans, S.J., Davies, J., Tarasick, D.W., Hoegger, B., Stubi, R., Schmidlin, F.J., Northam, T., Thompson, A.M., Witte, J.C., Boyd, I., Posny, F., 2007. Assessment of the performance of ECC ozonesondes under quasi-flight conditions in the environmental simulation chamber: insights from the Juelich Ozone Sonde Intercomparison Experiment (JOSIE). J. Geophys. Res. 112, D19306. https://doi.org/10.1029/2006JD007308.

Stergiopoulou, A., Katavoutas, G., Samoli, E., Dimakopoulou, K., Papageorgiou, I., Karagianni, P., Flocas, H., Katsouyanni, K., 2018. Assessing the associations of daily respiratory symptoms and lung function in schoolchildren using an Air Quality Index for ozone: results from the RESPOZE panel study in Athens, Greece. Sci. Total Environ., 492–499 https://doi.org/10.1016/j.scitotenv.2018.03.159.

Thomas, R.W.L., Holland, A.C., 1977. Ozone estimates derived from Dobson direct sun measurements: effect of atmospheric temperature variations and scattering. Appl. Opt. 16, 613–618. https://doi.org/10.1364/AO.16.000613.

Thompson, A.M., Witte, J.C., Smit, H.G.J., Oltmans, S.J., Johnson, B.J., Kirchhoff, V.W.J.H., Schmidlin, F.J., 2007a. Southern Hemisphere Additional Ozonesondes (SHADOZ) 1998–2004 tropical ozone climatology: 3. Instrumentation, station-to-station variability, and evaluation with simulated flight profiles. J. Geophys. Res. 112, D03304. https://doi.org/10.1029/2005JD007042.

Thompson, A.M., Stone, B.J., Witte, J.C., et al., 2007b. Intercontinental Chemical Transport Experiment Ozonesonde Network Study (IONS) 2004: 1. Summertime upper troposphere/lower stratosphere ozone over northeastern North America. J. Geophys. Res. 112, D12S12. https://doi.org/10.1029/2006JD007441.

Thompson, A.M., Stone, J.B., Witte, J.C., et al., 2007c. Intercontinental Chemical Transport Experiment Ozonesonde Network Study (IONS) 2004: 2. Tropospheric ozone budgets and variability over northeastern North America. J. Geophys. Res. 112, D12S13. https://doi.org/10.1029/2006JD007670.

Vömel, H., David, D.E., Smith, K., 2007. Accuracy of tropospheric and stratospheric water vapor measurements by the cryogenic frost point hygrometer: instrumental details and observations. J. Geophys. Res. 112, D08305. https://doi.org/10.1029/2006JD007224.

Wang, W.G., Fan, W.X., Wu, J., Xie, Y.Q., Yuan, M., Chen, X.M., Yang, Q., Wang, H.Y., 2006. A study of spatial-temporal evolvement of the global cross-tropopause ozone mass flux. Chin. J. Geophys. 49 (6), 1595–1607 (in Chinese).

Wang, W.G., Zuo, Q.J., Wang, H.Y., Fan, W.X., Bian, J.C., Peng, Y.Q., Li, X.J., 2010. The structure of O_3/H_2O mixing relationships in the tropopause transition layer in middle and high latitudes of the Northern Hemisphere. Chin. J. Geophys. 53 (6), 2805–2816 (in Chinese).

Wang, T., Xue, L.k., Brimblecombe, P., Lam, Y.F., Li, L., Zhang, L., 2017. Ozone pollution in China: a review of concentrations, meteorological influences, chemical precursors, and effects. Sci. Total Environ., 1582–1596 https://doi.org/10.1016/j.scitotenv.2016.10.081.

World Climate Research Programme, 1998. SPARC/IOC/GAWassessment of trends in the vertical distribution of ozone, stratospheric processes and their role in climate. Global Ozone Res. Monit. Proj. Rep. 43. World Meteorol. Organ., Geneva, Switzerland.

Yan, X.L., Zheng, X.D., Zhou, X.J., Holger, V., Song, J.Y., Li, W., Ma, Y.H., Zhang, Y., 2015. Validation of Aura Microwave imb Sounder water vapor and ozone profiles over the Tibetan Plateau and its adjacent region during boreal summer. Sci. China Earth Sci. 58, 589–603. https://doi.org/10.1007/s11430-014-5014-1.

Zheng, Y.G., Chen, L.Y., Chen, Z.Y., Cui, H., Zheng, X.D., Qin, Y., 2005. Comparison of characteristics of ozone vertical distribution above Lin. An, Kunming, and Hong Kong during spring 2001. Acta Sci. Nat. Univ. Pekin. 41 (1), 104–114. https://doi.org/10.13209/j.0479-8023.2005.016.

Zhou, X.J., Luo, C., Li, W.L., Shi, J.E., 1995. Changes in total ozone in China and low-value center in the Qinghai-Tibet Plateau. Chin. Sci. Bull. 40 (15), 1396–1398. https://doi.org/10.1360/csb1995-40-15-1396.